RESEARCH ARTICLE

The impact of aromatic amino acids on the thermal stability of xylanase XynXM

Chuanfeng Li[†], Jiatao Zhang[†], Yuanyuan Zhai, Ruilin Wang, Beibei Hua, Lele Xin, Qing Zhang, Tongbiao Li, Jinjin Zhu[*]

School of Biological Science and Food Engineering, Huanghuai University, Zhumadian, Henan, China.

Received: March 13, 2024; **accepted:** June 14, 2024.

As an industrial enzyme, xylanase has great potential in the food industry, pulp bleaching, feed production, and energy development. The poor thermal stability is an important factor, limiting its industrial application. Modification of enzyme molecules is one of the effective ways to improve the thermal stability of xylanase. To investigate the molecular mechanisms underlying the impact of aromatic amino acid integration on the thermal stability of xylanase, this study centered on XynXM sourced from *Aspergillus brunneoviolaceus* CBS 621.78 and employed FireProt predictions alongside site-directed mutagenesis. Five single-point mutants (G43P, S83W, N97F, T176Y, and N211F) were engineered with aromatic amino acids being introduced for each from distinct regions. Among these mutants, N97F and N211F, displaying heightened thermal stability, were chosen for further analysis. Relative to wild type XynXM, both mutants N97F and N211F manifested a noteworthy increase in optimal temperature by 10°C and 5°C, respectively. At 45°C, the half-life of N97F increased by 1.7-fold compared to that of wild type. Similarly, under the same conditions, N211F exhibited a marginally increased half-life of 62.6 min compared to that of the wild type (61.6 min). Notably, the combination mutant N97F/N211F exhibited a 1.4-fold increase in half-life at 50°C compared to the single mutant N97F. Molecular structure simulations conducted on the five single-point mutants and the combined mutant elucidated that aromatic amino acids within the enzyme were in close proximity to surrounding amino acids. Moreover, the side chains of aromatic amino acids were oriented toward the enzyme interior, thereby facilitating enhanced thermal stability. This study significantly contributed to the theoretical comprehension of xylanase thermal stability, offering valuable insights for molecular engineering approaches targeting other GH11 family xylanases.

Keywords: xylanase; FireProt; site-directed mutagenesis; thermal stability; aromatic amino acids.

[*]**Corresponding author:** Jinjin Zhu, School of Biological Science and Food Engineering, Huanghuai University, Zhumadian 463000, Henan, China. Email: hhz20190826@126.com.

[†]These authors contributed equally to this work.

Introduction

Xylan, a heterogeneous polysaccharide, primarily consists of arabinose and xylose linked by β-1,4-glycosidic bonds. It constitutes a significant fraction of plant hemicellulose, accounting for approximately 15% to 35% of the dry weight of plant cells [1, 2]. Xylanases, belonging to the glycoside hydrolase (GH) category, include both endo-β-1,4-xylanases and exo-β-1,4-xylanases. These enzymes catalyze the random hydrolysis of the β-1,4-glycosidic bonds in xylan, yielding functional low-molecular-weight xylooligo-saccharides such as xylobiose and xylotriose.

Xylanases are categorized into various families including GH5, GH7, GH8, GH10, GH11, and GH43 based on their structural, catalytic, and physicochemical characteristics with GH10 and GH11 families being the most prominent [3]. Xylanases are widely distributed in nature with numerous microorganisms including actinomycetes, fungi, and bacteria capable of producing them. Among these, xylanases derived from fungi and bacteria have been extensively studied. Serving as crucial biocatalysts, xylanases find wide-ranging applications across multiple industries including pulp bleaching, food processing, feed processing, textiles, and brewing [4, 5]. In feed processing, xylanase aids in the breakdown of non-starch polysaccharides (NSPS) into smaller oligosaccharides, thereby mitigating or eliminating the anti-nutritional effects caused by the high viscosity of NSPS in the animal gastrointestinal tract. This, in turn, improves feed performance while simultaneously contributing to the breakdown of plant cell wall structures, enhancing the activity of digestive enzymes in animals, and improving feed nutrient utilization [6].

For effective industrial application, xylanase, as a crucial industrial enzyme, necessitates high thermal stability. In industrial settings, heat-resistant xylanase can substantially reduce enzyme loading and microbial contamination, thereby enhancing production efficiency [7]. However, several highly active natural xylanases are mesophilic, exhibiting poor thermal stability, which hampers their industrial utility [8, 9]. Hence, enhancing the thermal stability of xylanase has become a paramount concern for researchers. To address this challenge, numerous researchers have conducted extensive studies. Li *et al*. conducted a rational design of the GH11 family xylanase PixA from *Penicillium janthinellum* MA21601. Strategies such as N-terminal substitution and the introduction of disulfide bonds in different regions led to a significant improvement in the thermal stability of xylanase PixA, laying the groundwork for its industrial application [10, 11]. Advancements in bioinformatics analysis methods and genetic engineering technologies have resulted in a more comprehensive exploration of mechanisms underlying xylanase thermal stability. Several factors were revealed to significantly influence the heat resistance of xylanase including the incorporation of aromatic amino acids including tyrosine, phenylalanine (Phe), and tryptophan (Trp) into the enzyme molecule. Aromatic amino acids possess a benzene ring structure, and their interactions play a pivotal role in protein stability maintenance [12]. Georis *et al*. reported the aromatic amino acid tyrosine in the mesophilic xylanase Xyl1, leading to an increase of 10°C in its optimal reaction temperature [13]. According to structural analysis, amino acids Y11 and Y16 were located on the β-folds B1 and B2 chains, respectively. The interactions between these amino acids improved the N-terminus stability of the xylanase.

However, the introduction of aromatic amino acids at various regions or sites can yield varying effects on enzyme structural stability and may even enhance thermal stability. This study employed the FireProt online server to predict potential beneficial mutants of the *Aspergillus brunneoviolaceus* CBS 621.78 xylanase XynXM. Five mutants incorporating aromatic amino acids were selected for thermal stability testing to elucidate the molecular mechanisms underlying the impact of introducing aromatic amino acids on xylanase thermal stability. This study provided novel approaches for molecular engineering to enhance the thermal stability of other xylanases. Further, obtaining xylanase mutants with improved thermal stability could enhance the applicability of the enzyme for industrial purposes.

Materials and methods

Recombinant xylanase XynXM homology modeling and mutant site design

The amino acid sequence of the recombinant xylanase XynXM was submitted to SWISS-MODEL (https://swissmodel.expasy.org/) for homology modeling. Further optimization was facilitated

Table 1. The mutagenic primer sequences.

Primer name	Sequences (5'— 3')
G43P-F	GCT GAG CGC TCG ACT CCT AGC TCC ACT GGC TAC
G43P-R	GTA GCC AGT GGA GCT AGG AGT CGA GCG CTC AGC
S83W-F	ACC TGG TCA TCG GCC TGG AAC TTC GTC GGT GGA
S83W-R	TCC ACC GAC GAA GTT CCA GGC CGA TGA CCA GGT
N97F-F	AAC CCT GGA AGT GCT TTT GAC ATT ACG TAC TCC
N97F-R	GGA GTA CGT AAT GTC AAA AGC ACT TCC AGG GTT
T176Y-F	GGC ACG GCC ACT TTC TAC CAG TAC TGG TCC ATT
T176Y-R	AAT GGA CCA GTA CTG GTA GAA AGT GGC CGT GCC
N211F-F	AAT CTG GGC ACG CAC TTT TAT CAG ATC GTC GCT
N211F-R	AGC GAC GAT CTG ATA AAA GTG CGT GCC CAG ATT

Note: Base mutation sites are underlined.

using Discovery Studio (BIOVIA, San Diego, CA, USA) to analyze the molecular interactions within the enzyme structure. The optimized XynXM structure model was then subjected to FireProt (https://loschmidt.chemi.muni.cz/fireprot/) to predict potential thermostable mutants. The enzyme structure was visualized using PyMOL (Schrödinger, New York, NY, USA).

Site-directed mutagenesis

A rapid site-directed mutagenesis strategy was employed [14], and mutagenic primers were designed (Table 1). The recombinant plasmid pET-28a-xynXM was utilized as the template for polymerase chain reaction (PCR) amplification using mutagenic primers. The mutated plasmid was constructed following the instructions of the Fast Mutagenesis Kit (Vazyme, Nanjing, Jiangsu, China). The resultant recombinant mutated plasmid was then chemically transformed into *E. coli* DH5α (Novagen, Madison, WI, USA) competent cells. After screening for kanamycin resistance, positive monoclonal clones were selected and sent to Sangon Biotech (Shanghai, China) for gene sequencing. The recombinant plasmid of the single-site mutant was used as the template for constructing double-site recombinant mutant plasmids using the same methods.

Recombinant xylanase expression and purification

The accurately sequenced recombinant mutant plasmids were chemically transformed into *E. coli* BL21 (Novagen, Madison, WI, USA) competent cells to generate genetically engineered bacteria. Positive monoclonal clones were selected and inoculated into 3 mL lysogeny broth with 50 μg/mL of kanamycin for overnight incubation at 37°C under shaking conditions of 180 rpm. The culture was then transferred to Terrific broth and incubated at 37°C under shaking conditions at 180 rpm until the OD at 600 nm reached 0.6 - 0.8. IPTG (Sangon Biotech (Shanghai) Co, Ltd., Shanghai, China) was added to a final concentration of 2 mM, and induction continued for 2 h at 30°C. The cells were disrupted following induction, and the supernatant containing the crude enzyme was collected [15]. The recombinant xylanase was purified using the Ni-NTA protein purification kit (Sangon Biotech (Shanghai) Co, Ltd., Shanghai, China) following the manufacturer's instructions. The purity of the recombinant xylanase was analyzed using sodium dodecyl-sulfate polyacrylamide gel electrophoresis (SDS-PAGE) with 10% separating gel and 5% concentrating gel. Protein concentration was determined using the Bradford method [16].

Recombinant xylanase activity assay

Xylanase activity was assessed utilizing the 3,5-Dinitrosalicylic acid (DNS) method [17]. Briefly, a reaction mixture comprising 1.5 mL of 0.5% birchwood xylan and 1 mL of appropriately

diluted enzyme solution was incubated at a serious temperature for 15 min. The reaction was halted by the addition of 2.5 mL DNS followed by boiling for 7 min. After cooling, the absorbance was measured at 540 nm. Xylanase activity was quantified in units (U) and defined as the amount of enzyme required to liberate 1 µmol of xylose per min under the specified conditions.

Temperature and pH characteristics of recombinant xylanase

The determination of xylanase activity was conducted using the DNS method at temperatures ranging from 35 - 60°C for 15 min to establish the optimum temperature. The relative enzyme activity at other temperatures was computed relative to the maximum activity observed. The residual enzyme activity of the recombinant xylanase was evaluated post-incubation at 45°C, 50°C, and 55°C for 60 min using the DNS method. The relative residual enzyme activity was calculated with respect to the untreated enzyme to assess thermal stability. The enzyme activity half-life was evaluated following the method outlined by You *et al*. [18]. The optimal pH was ascertained at the optimal reaction temperature for wild type XynXM and mutants within a pH range of 4.0 – 9.0. Following a 1 h incubation at 40°C under various pH conditions, the residual enzyme activity was measured, and relative residual enzyme activity was calculated.

Statistical analysis

Each experiment was conducted with three replicates, and the data were averaged. GraphPad Prism 5.0 software (https://www.graphpad.com/) was used to perform statistical analysis and graphical representation.

Results

Construction of high-quality recombinant xylanase XynXM structural model

Prior research has highlighted that the accuracy of homology modeling for the three-dimensional structure of a target protein is largely contingent upon the level of homology with the primary structure of the template protein. When the homology surpasses 60%, the modeled structure closely approximates the actual crystal structure of the protein. For homology modeling of xylanase XynXM, BmGH11, a GH11 family xylanase with the highest homology (70.1%) in the Protein Data Bank (PDB) database (PDB No. 8b8e) was opted as the template. Homology modeling was conducted using SWISS-MODEL, and subsequent refinement of the XynXM structure model was carried out using Discovery Studio. XynXM exhibited a typical GH11 family xylanase structure, characterized by an α-helix and two antiparallel β-folded sheets, forming a right-handed half-handshake structure (Figure 1).

Figure 1. The structural model of XynXM.

Screening of mutation sites

In the preliminary phase, the structural model of XynXM was submitted to FireProt, resulting in the prediction of 17 potential thermostable mutants. The FireProt results were presented in Table 2 [19], and available on the website https://loschmidt.chemi.muni.cz/fireprotweb/?action=calculation&job=xlmhmz. Concurrently,

Table 2. Prediction of the potential thermal stability mutants of XynXM.

Combined mutant:				-22.01 kcal/mol (17 mutations)			
Chain	**Mutation**	**Conserved**	**Correlated**	**BTC by majority**	**BTC by ratio**	**FoldX (kcal/mol)**	**Rosetta (kcal/mol)**
B	G43P	N	N	N	Y	0.44	
B	T58C	N	N	N	N	-1.17	-3.99
B	E66T	N	N	Y	Y	0.05	
B	S68T	N	N	Y	Y	0.01	
B	S83W	N	N	Y	Y	-1.65	-3.52
B	N97F	N	N	N	N	-2.12	-2.04
B	D98T	N	N	N	N	-0.28	
B	V126I	N	N	Y	Y	-0.10	
B	E136T	N	N	Y	N	0.16	
B	A142G	N	N	Y	N	-0.14	
B	G143W	N	N	N	N	-2.63	-6.26
B	S148T	N	N	Y	N	-0.00	
B	N157D	N	N	Y	N	0.36	
B	T176Y	N	N	N	N	-1.09	-2.73
B	T184S	N	N	N	Y	0.25	
B	A201L	N	N	N	N	-1.10	-7.32
B	N211F	N	N	N	N	-1.03	-3.01

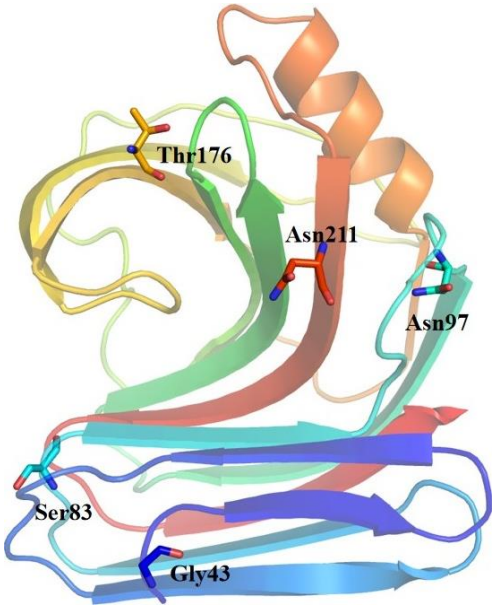

Figure 2. Spatial distribution of the mutation sites containing aromatic amino acid substitutions in XynXM.

the predicted G143W mutant was experimentally validated, which exhibited a notable improvement in thermal stability compared to that of the wild type. Structural analysis revealed that the introduction of the aromatic amino acid Trp in the cord structure played a pivotal role in increasing the thermal stability of the G143W mutant. Examination of the predictions of FireProt for xylanase XynXM indicated that mutants with aromatic amino acid substitutions were predicted in the N-terminal loop region, β-folds, and the regions connecting β-folds, including G43P, S83W, N97F, T176Y, and N211F (Table 2 and Figure 2). Hence, based on these predictions, the corresponding mutants were constructed to explore the effect of introducing aromatic amino acids in different regions on the thermal stability of XynXM.

Construction and characterization of xylanase single-point mutants

Five mutants including G43P, S83W, N97F, T176Y, and N211F were generated employing the rapid site-directed mutagenesis strategy. The electrophoresis results showed that both wild type XynXM and mutants G43P, S83W, N97F, T176Y, and N211F exhibited distinct bands at approximately 27 kDa, indicating the high purity of the purified protein samples suitable for enzymatic property analysis (Figure 3). After incubation at 50°C for 30 min, the enzymatic

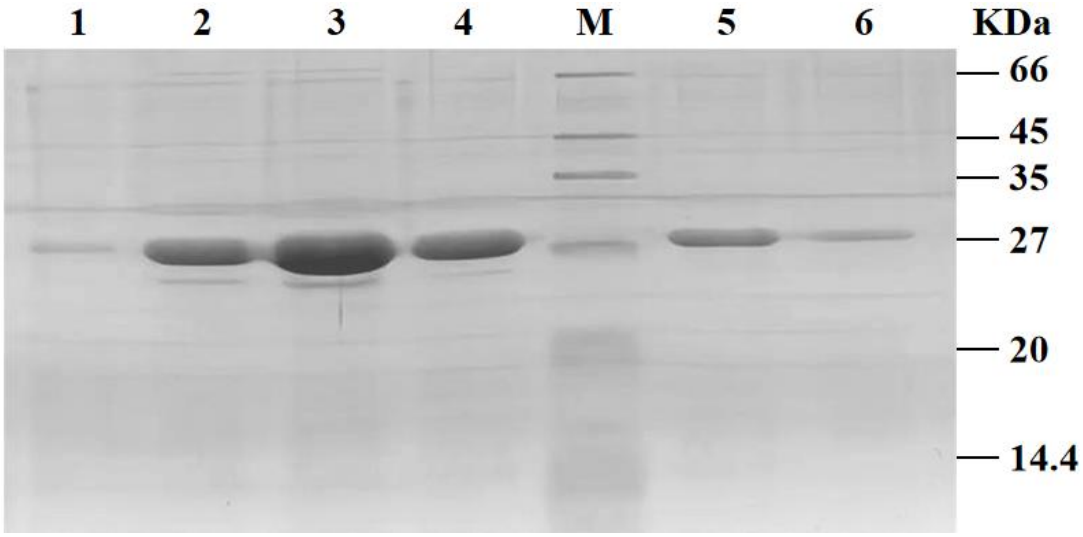

Figure 3. SDS-PAGE analysis of the purified recombinant xylanases. **M:** protein marker. **Lane 1:** mutant S83W. **Lane 2:** mutant N97F. **Lane 3:** mutant T176Y. **Lane 4:** mutant N211F. **Lane 5:** wild type XynXM. **Lane 6:** mutant G43P.

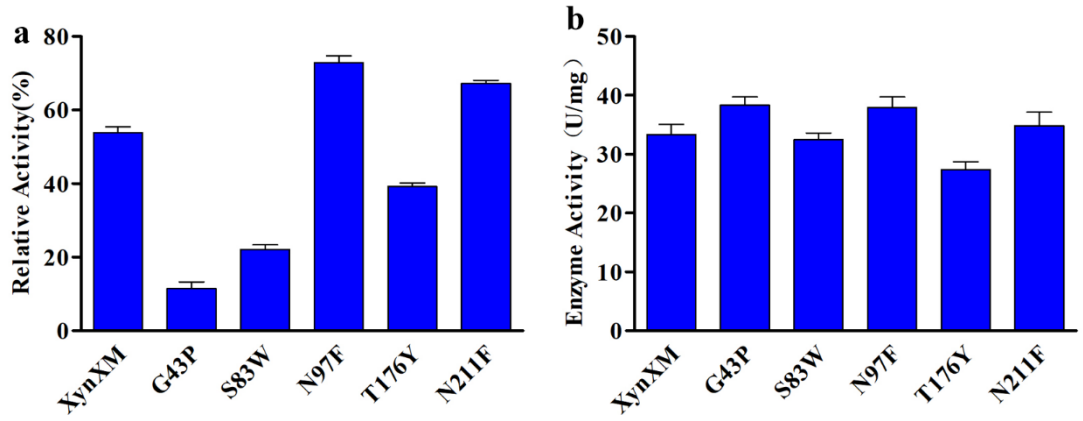

Figure 4. Characterization of wild type and single mutants. **a.** The residual enzyme activity of recombinant xylanases after incubating at 50°C for 30 min and then measuring at 50°C. **b.** Specific enzyme activity of crude recombinant xylanases.

activities of mutants G43P, S83W, and T176Y decreased by 42.4%, 31.8%, and 14.6% compared to wild type, respectively, indicating significantly decreased thermal stability in these three mutants. However, under the same conditions, mutants N97F and N211F displayed relative enzyme activities of 72.9% and 67.2%, respectively, revealing considerably improved heat resistance compared to wild type XynXM (53.9%) (Figure 4a). Furthermore, the specific enzyme activities of crude extracts from the single-point mutants were measured, and these mutants retained enzyme activities similar to the wild type XynXM. Mutants N97F and N211F exhibited slightly higher specific enzyme activities of 37.9 U/mg and 34.9 U/mg, respectively than that of 33.4 U/mg in wild type XynXM (Figure 4b).

Temperature and pH characteristics of single-point mutants

The optimal temperatures for the single-point mutants N97F and N211F were determined across a temperature range of 35 to 60°C. While wild type XynXM exhibited an optimal temperature of 45°C, mutants N97F and N211F

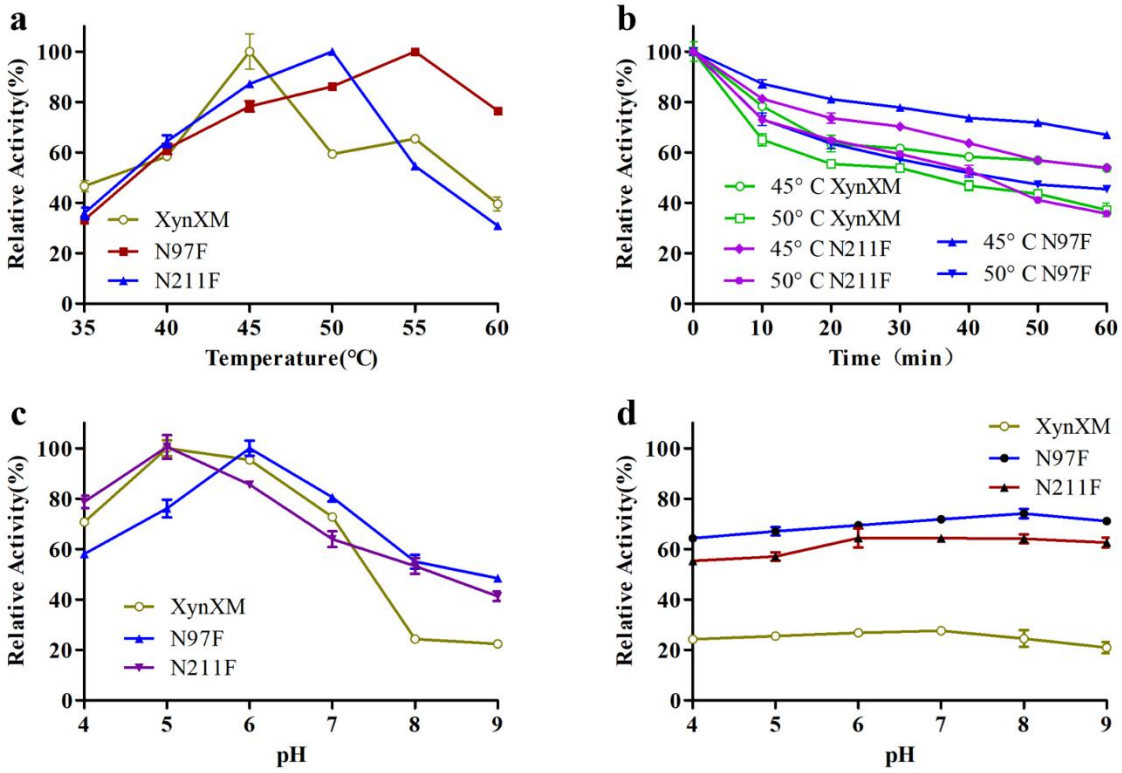

Figure 5. Effect of temperature and pH on the stability for wild type and single mutants. **a.** Optimal temperature of wild type and single mutants. **b.** Thermostability of wild type and single mutants. **c.** Optimum pH of wild type and single mutants. **d.** pH stability of wild type and single mutants.

demonstrated optimal temperatures of 55°C and 50°C, respectively, reflecting 5°C and 10°C increases compared to that of wild type XynXM (Figure 5a). To evaluate the thermal stability of the mutants, residual enzyme activity was measured after incubation at 45°C and 50°C for 1 h (Figure 5b). Both mutants N97F and N211F exhibited enhanced heat resistance compared to that of wild type XynXM. Following incubation at 45°C for 30 min, the enzyme activities of mutants N97F and N211F reached 77.8% and 70.3%, respectively, whereas wild type XynXM retained only 61.6% enzyme activity. Furthermore, after 1 h at 45°C, mutant N97F maintained over 60% enzyme activity, whereas wild type XynXM dropped to approximately 50%. After 1 h at 50°C, mutant N97F exhibited an enzyme activity of 45.5%, representing an improvement over wild type XynXM (37.2%). Determination of the half-life at 45°C revealed that wild type XynXM had a half-life of 61.6 min, whereas mutant N97F displayed a half-life of 106.8 min, marking a 1.7-fold increase. Under the same conditions, mutant N211F exhibited a slightly increased half-life of 62.6 min. At 50°C, the half-lives of wild type XynXM, mutant N97F, and mutant N211F were 41.5, 46.5, and 39.8 min, respectively. Notably, mutant N97F exhibited an extended half-life compared to that of wild type at 50°C (Figure 5b). These findings suggested that substituting the amino acid residues Asn97 and Asn211 with the aromatic amino acid Phe could effectively improve the thermal stability of the XynXM enzyme. Regarding the determination of optimal pH values, the pH range of 4.0 - 9.0 was examined. Wild type XynXM exhibited an optimal pH of 5.0, whereas mutant N211F retained the same optimal pH (Figure 5c). However, mutant N97F displayed an optimal pH 1 unit higher than that of wild type. In pH stability testing, mutants N97F and N211F exhibited significant improvements compared to that of wild type, maintaining enzyme activity above 60% after incubation at 40°C for 1 h (pH: 4.0 - 9.0). In

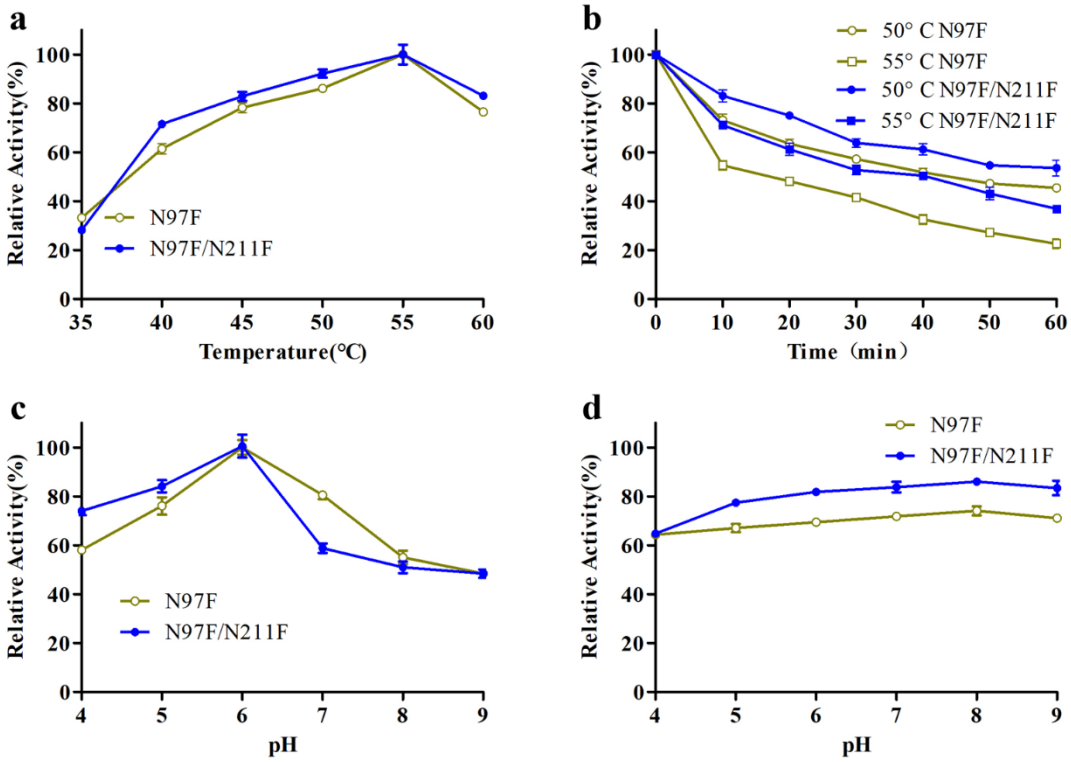

Figure 6. Effect of temperature and pH on the stability of the mutants. **a.** Optimal temperature of the mutants. **b.** thermostability of the mutants. **c.** Optimum pH of the mutants. **d.** pH stability of the mutants.

contrast, under the same pH conditions, wild type XynXM exhibited enzyme activity between 20% and 30% (Figure 5d). These results suggested that mutants N97F and N211F possessed higher pH resistance than that of wild type.

Temperature and pH characteristics of double-point mutants

To explore the combined effects of double-point mutations, the mutant N97F/N211F was constructed through site-directed mutagenesis. Given the higher thermal stability demonstrated by the N97F single-point mutant compared to both wild type and N211F, N97F was used as a reference to analyze the temperature and pH characteristics of the double-point mutant N97F/N211F. The optimal temperature of mutant N97F/N211F remained consistent with that of wild type at 55°C (Figure 6a). Further investigation into the thermal stability of the combined mutant revealed higher residual enzyme activity compared to that of single-point mutant N97F after incubation at 50°C and 55°C for 1 h (Figure 6b). At 50°C, the mutant N97F/N211F retained 53.6% activity after 1 h, whereas the single-point mutant N97F dropped to 45.5%. Similarly, at 55°C, while the enzyme activity of mutant N97F decreased to 22.6%, the mutant N97F/N211F still maintained 36.9% enzyme activity. The half-life of mutant N97F/N211F at 50°C was 62.8 min, indicating a 1.4-fold increase compared to 46.5 min of N97F and a 1.5-fold increase compared to 41.5 min of wild type XynXM. Additionally, at 55°C, the half-life of mutant N97F/N211F was 38.1 min, a 1.7-fold increase compared to 22.2 min of N97F (Table 3). These results demonstrated a significant enhancement in thermal stability for the combined mutant N97F/N211F compared to that of both single-point mutant and wild type XynXM. The enzyme activities of the double-point mutant N97F/N211F at different pH values (4.0 – 9.0) were also evaluated (Figures 6c and 6d). The optimal pH of mutant N97F/N211F

Table 3. Summary of properties of XynXM and its mutants.

	Optimum temperature (°C)	Half-life at 45°C (min)	Half-life at 50°C (min)	Half-life at 55°C (min)
XynXM	45	61.6	41.5	—
N97F	55	106.8	46.5	22.2
N211F	50	62.6	39.8	—
N97F/N211F	55	—	62.8	38.1

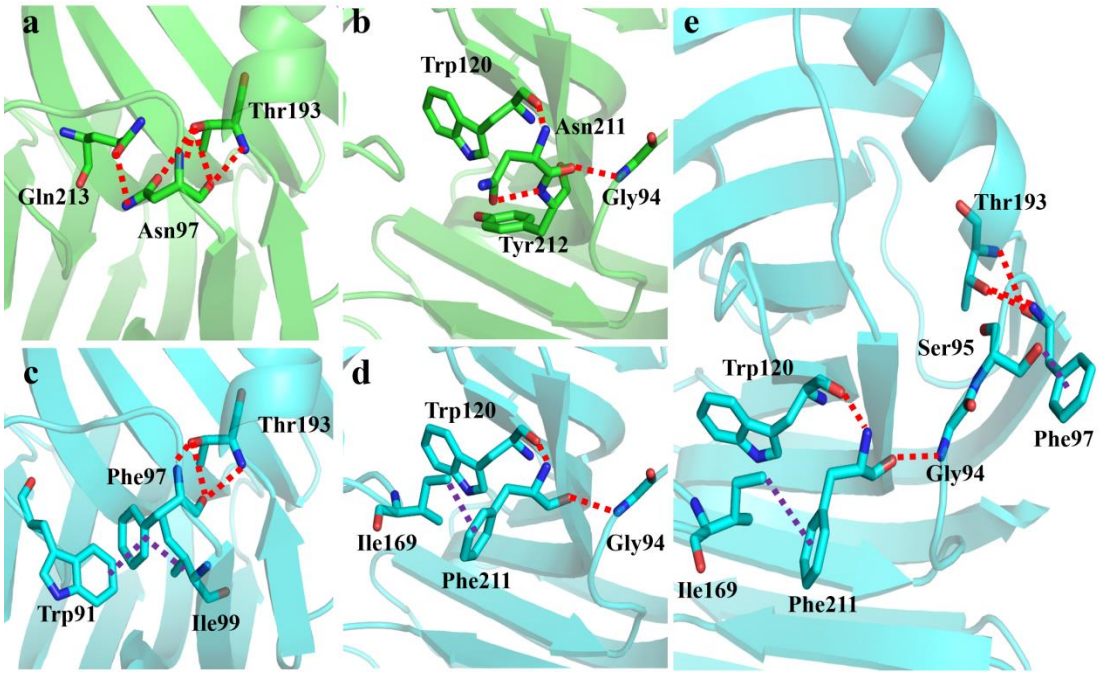

Figure 7. Intramolecular interactions of wild type (a, b), mutant N97F (c), N211F (d), and N97F/N211F (e) residues predicted by Discovery Studio. The color of each interaction type was defined as purple represented hydrophobic contacts, while red represented hydrogen bonds.

remained consistent with the single-point mutant N97F. Testing of pH stability demonstrated that, after incubation at 40°C for 1 h within the pH range of 5.0 – 8.0, the mutant N97F/N211F retained approximately 80% of its enzyme activity, indicating a significant improvement in pH stability compared to that of single-point mutant N97F.

Structural analysis of xylanase mutants

Previous studies have highlighted the role of hydrogen bonds and hydrophobic interactions in stabilizing protein structures, thus enhancing thermal stability of xylanase [20 - 22]. Therefore, the alterations in hydrogen bonds and hydrophobic interactions were analyzed following key amino acid residue mutations. Using wild type XynXM as a reference, the homology modeling was performed for mutants N97F, N211F, and N97F/N211F. In wild type XynXM, Asn97 formed one hydrogen bond with the spatially adjacent Gln213 and four hydrogen bonds with Thr193. However, in the N97F mutant, due to the substitution of Asn97 with Phe, the side-chain interactions were altered. The number of hydrogen bonds between Phe97 and Thr193 decreased to three, and the hydrogen bond with Gln213 disappeared. Instead, Phe97 established hydrophobic interactions with Trp91 and Ile99, respectively (Figures 7a vs. 7c). Similarly, in the N211F mutant, Asn211 in wild type XynXM formed hydrogen

bonds with Gly94, Trp120, and Tyr212. However, in the N211F mutant, the hydrogen bond with Tyr212 vanished and was replaced by hydrophobic interactions between Phe211 and Ile169. The locations where Phe211 formed hydrogen bonds and interacted with other residues remained consistent with wild type XynXM (Figures 7b vs. 7d). Compared to wild type XynXM, in mutants N97F and N211F, the introduction of the aromatic amino acid Phe led to the disappearance of certain hydrogen bonds between mutated residues and adjacent residues, which were replaced by hydrophobic interactions. The results suggested that, in these mutants, hydrophobic interactions might play a more significant role in stabilizing the internal structure of the protein than hydrogen bonds, thereby enhancing the thermal stability of the enzyme. Structural analysis of the double-point mutant N97F/N211F unveiled changes resulting from the simultaneous mutations of N97F and N211F. The hydrophobic interactions between Phe97 - Trp91 and Phe97 - Ile99 in the N97F mutant vanished, but Phe97 established a hydrophobic interaction with Ser95. Other intermolecular forces remained consistent with mutants N97F and N211F (Figure 7e). The results suggested that the double-point mutation in N97F/N211F improved the molecular interactions observed in the single-point mutants N97F and N211F, further bolstering the protein structure stability and promoting the improved thermal stability of the combined mutant.

Discussion

Xylanase plays an important role in catalyzing the breakdown of wood cellulose into functional low oligosaccharides, including xylose, xylobiose, and xylotriose. This enzymatic activity contributes to reducing industrial production costs and improving efficiency [23-25]. Although many research directions and methods are available for modifying wood cellulase, the complexity and diversity of wood cellulase present considerable challenges in industrial applications, particularly in improving its thermal stability, which can increase economic efficiency [26, 27]. Only a limited amount of highly thermally stable wood cellulases are found in nature. Nevertheless, protein engineering techniques and molecular simulation technologies have facilitated the rapid development of mutant wood cellulases with improved thermal stability [28, 29]. The recently developed online server, FireProt, uses three enzyme engineering strategies and 16 protein structure calculation tools for the quick and effective design of protein thermal stability. This software uses strategies based on both energy and evolution to design single-point mutations. The server also employs a rational combination strategy to predict multi-point mutants [30]. FireProt has successfully contributed to improving the thermal stability of different enzymes, such as monooxygenase [31], serine protease [32], nitrile hydratase [33], and carbonyl reductase [34].

Previous studies have shown that adding aromatic amino acids into enzyme molecules is an effective approach for improving thermal stability [35, 36]. This study aimed to gain a deeper understanding of the molecular mechanisms underlying the effect of aromatic amino acids on the thermal stability of GH11 recombinant wood cellulase XynXM. Based on the results of the FireProt web server, five mutants with aromatic amino acid substitutions in XynXM were selected, namely G43P, S83W, N97F, T176Y, and N211F. Initial screening for thermal stability involved treating mutants at 50°C for 30 min, which led to a significant decrease in residual enzyme activity and thermal stability of mutants G43P, S83W, and T176Y compared with the wild type XynXM. Conversely, mutants N97F and N211F showed improved thermal stability under the same incubation conditions. The thermal stability of the single-point mutants N97F and N211F were then determined along with the combined mutant N97F/N211F, revealing an additive effect in the improved thermal stability of N97F and N211F. Based on these findings, the molecular structure of the enzyme was simulated and the beneficial interactions between mutant residues were

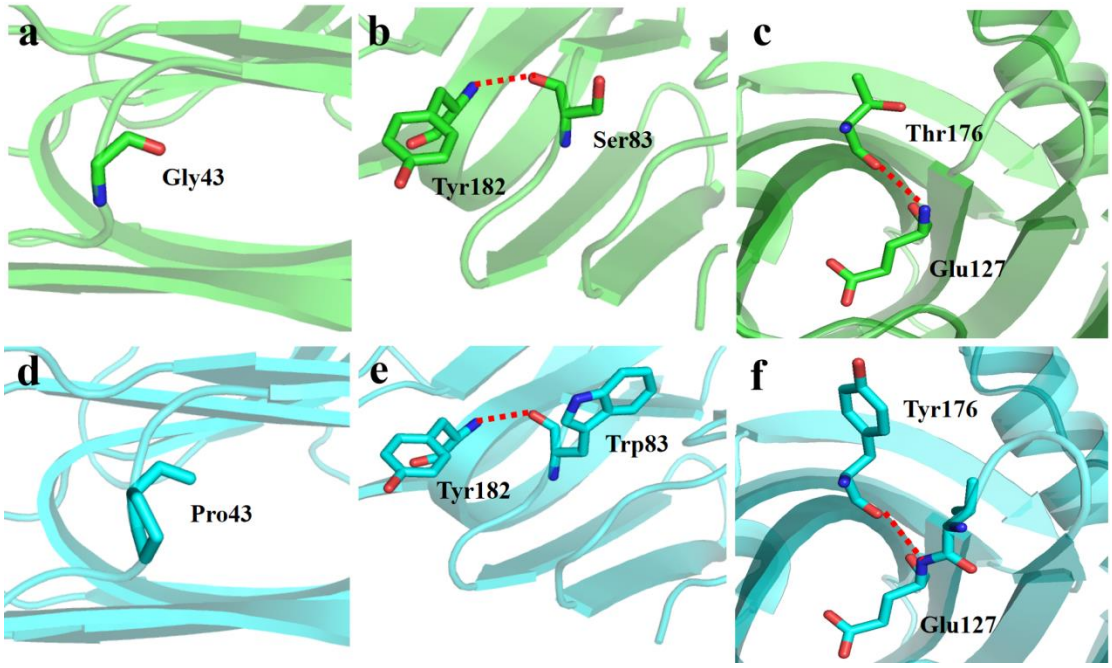

Figure 8. Intramolecular interactions of wild type (**a**, **b**, **c**), mutant G43P (**d**), S83W (**e**), and T176Y (**f**) residues predicted by Discovery Studio. The color of each interaction type was defined as purple represented hydrophobic contacts, while red represented hydrogen bonds.

analyzed, which warranted the study of multi point mutants in future.

Aromatic amino acids play an important role in improving the thermal stability of enzyme molecules due to their bulky side-chain groups, facilitating the formation of more hydrogen bonds or hydrophobic interactions with spatially adjacent amino acid residues, which, in turn, improves the overall stability of the enzyme molecule [37, 38]. All five selected single-point mutants involved substitutions with aromatic amino acids. However, noticeable differences in the thermal stability of each mutant were identified. In the G43P mutant, Pro43 was introduced into the N-terminal Loop region. The Discovery Studio software revealed that Gly43 in wild type XynXM did not form hydrogen bonds or hydrophobic interactions with neighboring amino acid residues. Substituting Gly43 with the larger sidechain of Pro43 could not establish interactions with neighboring amino acids. Subsequent analysis of the structure of both wild type XynXM and the G43P mutant showed that the 43rd position was in the flexible N-terminal loop region, which was characterized by high flexibility and was considerably distant from other amino acids in the enzyme molecule. Even if the aromatic amino acid Pro was added at this position, achieving the required distance for hydrogen bonding or hydrophobic interactions was difficult (Figures 8a and 8d). Consequently, the distance between the added aromatic amino acid and the neighboring amino acids was considered a vital factor for improving the stability of the enzyme molecule. Furthermore, Pro43 could interact with water molecules when it was exposed to the external aqueous environment, aggravating the unfolding of the enzyme molecule and consequently reducing the thermal stability of the G43P mutant.

In wild type XynXM, the 83rd position was situated in the β-folded region, connecting adjacent structural elements, which was in close proximity with the neighboring amino acids, wherein Ser83 formed a hydrogen bond exclusively with Tyr182. However, in the S83W mutant, the substitution of Ser83 with Trp83 retained the large side chain that formed a

hydrogen bond exclusively with Tyr182 and did not induce additional hydrophobic interactions or hydrogen bonds. Despite the proximity of the 83rd position with the neighboring amino acids, the outward orientation of the Trp83 side chain inhibited interactions with internal amino acid residues (Figures 8b and 8e). Additionally, the exposure of Trp83 to the external aqueous environment decreased the thermal stability of the S83W mutant. This situation was further confirmed in the poorly heat-resistant T176Y mutant. The Tyr176 side chain in the T176Y mutant was located in the β-folded region and was oriented outward. Therefore, it was exposed to the external aqueous environment and formed hydrogen bonds with neighboring amino acids, which was similar to wild type XynXM (Figures 8c and 8f).

Conversely, mutants N97F and N211F exhibited considerable differences in intermolecular forces compared with mutants G43P, S83W, and T176Y (Figure 7). The Phe97 in mutant N97F was situated in the β-folded region, connecting adjacent structural elements, which was similar to Trp83 in S83W mutant. The Phe211 in mutant N211F was situated in the β-folded region, similar to the spatial position of Trp83 in T176Y mutant. Nevertheless, mutants N97F and N211F exhibited a considerable improvement in thermal stability. The spatial structural analysis of these two mutants revealed that mutant N97F and Phe97 and Phe211 in mutant N211F had side chains directed towards the interior of the enzyme molecule, which were in close proximity with the neighboring amino acids, and the aromatic amino acids formed due to the mutations exhibited stronger hydrophobic interactions with neighboring amino acids. This, in turn, stabilized the structure of the enzyme molecule and improved its thermal stability. The results showed that aromatic amino acids could improve the structural stability and thermal stability of enzymes when their side chains were near the neighboring amino acids within the enzyme molecule and oriented towards its interior.

Conclusion

This study adopted a strategy based on the substitution of aromatic amino acids to construct five single-point mutants of xylanase, namely G43P, S83W, N97F, T176Y, and N211F. Heat tolerance screening revealed that mutants N97F and N211F had improved thermal stability, exhibiting an increase in 10°C and 5°C in their optimal temperatures, respectively, compared with that of wild type. The half-life at 45°C increased from 61.6 min to 106.8 min for mutant N97F and from 61.6 min to 62.6 min for mutant N211F. The combined mutant N97F/N211F exhibited a synergistic effect, and its half-life at 50°C increased from 41.5 min for wild type to 62.8 min. At 55°C, the half-life of N97F/N211F increased considerably from 22.2 min for the single-point mutant to 38.1 min, suggesting a substantial improvement in thermal stability. Furthermore, mutants N97F, N211F, and N97F/N211F exhibited a considerable increase in pH stability compared with that of wild type. Moreover, molecular simulations of the mutant structures showed that the position and orientation of aromatic amino acids within the enzyme molecule considerably affected the thermal stability of xylanase.

Acknowledgements

This study was financially supported by the Foundation of Science and Technology Development Project of Henan Province (Grant No. 242102111041), Natural Science Foundation of Henan Province (Grant No. 242300421582), Key Scientific Research Projects of Colleges and Universities of Henan Province (Grant No. 22A180022).

References

1. Wang YW, Fu Z, Huang HQ, Zhang HS, Yao B, Xiong HR, *et al*. 2012. Improved thermal performance of *Thermomyces lanuginosus* GH11 xylanase by engineering of an N-terminal disulfide bridge. Bioresour Technol. 112:275-279.

2. Miao H, Zhao Y, Ma Y, Han N, Zhe Y, Tang X. 2021. Improving the thermostability of a fungal GH11 xylanase *via* fusion of a submodule (C2) from hyperthermophilic CBM9_1-2. Int J Mol Sci. 23(1):463.
3. Juturu V, Wu JC. 2012. Microbial xylanases: Engineering, production and industrial applications. Biotechnol Adv. 30:1219-1227.
4. Han NY, Ma Y, Mu YL, Tang XH, Li JJ, Huang ZX. 2019. Enhancing thermal tolerance of a fungal GH11 xylanase guided by B-factor analysis and multiple sequence alignment. Enzyme Microb Technol. 131:109422.
5. Abdo AAA, Zhang C, Lin Y, Liang X, Li WW. 2021. Xylo-oligosaccharides ameliorate high cholesteroldiet induced hypercholesterolemia and modulate sterol excretion and gut microbiota in hamsters. J Funct Foods. 77:104334.
6. Sun BG, Xu YQ, Xiong K, Teng C, Li XT. 2017. Improving special hydrolysis characterization into *Talaromyces thermophilus* F1208 xylanase by engineering of N-terminal extension and site-directed mutagenesis in C-terminal. Int J Biol Macromol. 96:451-458.
7. van Gool MP, van Muiswinkel GCJ, Hinz SWA, Schols HA, Sinitsyn AP, Gruppen H. 2012. Two GH10 endo-xylanases from *Myceliophthora thermophila* C1 with and without cellulose binding module act differently towards soluble and insoluble xylans. Bioresour Technol. 119:123-132.
8. Yan S, Xu Y, Yu XW. 2021. Rational engineering of xylanase hyper-producing system in *Trichoderma reesei* for efficient biomass degradation. Biotechnol Biofuels. 14:1-17.
9. Zouar AD, Hmida SA, Hajer BH, Sameh BM, Monia M, Samir B. 2015. Improvement of *Trichoderma reesei* xylanase II thermal stability by serine to threonine surface mutations. Int J Biol Macromol. 72:163-170.
10. Xiong K, Hou J, Jiang YF, Li XT, Teng C, Li O, *et al*. 2019. Mutagenesis of N-terminalresidues confer thermostability on a *Penicillium janthinellum* MA21601 xylanase. BMC Biotechnol. 19(1):1-9.
11. Teng C, Jiang YF, Xu YQ, Li Q, Li XT, Fan GS, *et al*. 2019. Improving the thermostability and catalytic efficiency of GH11 xylanase PixA by adding disulfidebridges. Int J Biol Macromol. 128:354-362.
12. Li XQ, Wu Q, Hu D, Wang R, Liu Y, Wu MC, *et al*. 2017. Improving the temperature characteristics and catalytic efficiency of a mesophilic xylanase from *Aspergillus oryzae*, AoXyn11A, by iterative mutagenesis based on in silico design. AMB Express. 7(1):97.
13. Georis J, de Lemos Esteves F, Lamotte-Brasseur J, Bougnet V, Devreese B, Giannotta F, *et al*. 2000. An additional aromatic interaction improves the thermostability and thermophilicity of a mesophilic family 11 xylanase: structural basis and molecular study. Protein Sci. 9(3):466-475.
14. Serradella VD, John WR. 2012. Conformation analysis of a surface loop that controls active site access in the GH11 xylanase A from *Bacillus subtilis*. J Mol Model. 18:1473-1479.
15. Xiong K, Hou J, Jiang YF, Li XT, Teng C, Li O, *et al*. 2019. Mutagenesis of N-terminal residues confer thermostability on a *Penicillium janthinellum* MA21601 xylanase. BMC Biotechnol. 19(1):1-9.
16. Bhat S, Purushothaman K, Kini K, Rao AGRA. 2021. Design of mutants of GH11 xylanase from *Bacillus pumilus* for enhanced stability by amino acid substitutions in the N-terminal region: an *in silico* analysis. J Biomol Struct Dyn. 40(17):7666-7679.
17. Li GQ, Chen XJ, Zhou X, Huang R, Zhang RF. 2019. Improvement of GH10 family xylanase thermostability by introducing an extra a-helix at the C-terminal. Biochem Biophys Res Commun. 515(3):417-422.
18. You C, Huang Q, Xue H, Yang X, Lu H. 2010. Potential hydrophobic interaction between two cysteines in interior hydrophobic region improves thermostability of a family 11 xylanase from *Neocallimastix patriciarum*. Biotechnol Bioeng. 105(5):861-870.
19. Li TB, Tang JZ, Li SQ, Peng H, Zhu YY, Zhu J, *et al*. 2022. Improving the thermostability of GH11 xylanase XynXM from *Aspergillus brunneoviolaceus* CBS 621.78 by the design of cord region. J Biotech Res. 13:130-141.
20. Li JF, Gao SJ, Liu XT, Gong YY, Wu MC. 2013. Modified pPIC9K vector-mediated expression of a family 11 xylanase gene, Aoxyn11A, from *Aspergillus oryzae* in *Pichia pastoris*. Ann Macrobiol. 63(3):1109-1120
21. Madhavan A, Arun KB, Binod P, Sirohi R, Tarafdar A, Reshmy R, *et al*. 2021. Design of novel enzyme biocatalysts for industrial bioprocess: Harnessing the power of protein engineering, high through put screening and synthetic biology. Bioresource Technol. 325:124617.
22. Vieira DS, Léo Degrève. 2009. An insight into the thermostability of a pair of xylanases: The role of hydrogen bonds. Mol Phys. 107(1):59-69
23. Zhang S, He YZ, Yu HY, Dong ZY, Danilo R. 2014. Seven N-terminal residues of a thermophilic xylanase are sufficient to confer hyperthermostability on its mesophilic counterpart I. PLoS One. 9(1):e87632.
24. Teng C, Tang H, Li X, Zhu Y, Fan G, Yang R. 2021. Production of xylo-oligosaccharides using a *Streptomyces rochei* xylanase immobilized on Eudragit S-100. Biocatal Biotransfor. 39:408-417.
25. Li X, Zhang L, Jiang ZT, Liu L, Wang JH, Zhong LL, *et al*. 2022. A novel cold-active GH8 xylanase from cellulolytic myxobacterium and its application in food industry. Food Chem. 393:133463.
26. Bhat S, Purushothaman K, Kini K, Rao AGRA. 2021. Design of mutants of GH11 xylanase from *Bacillus pumilus* for enhanced stability by amino acid substitutions in the N-terminal region: An *in silico* analysis. J Biomol Struct Dyn. 40(17):7666-7679.
27. Wu XY, Zhang Q, Zhang LZ, Liu SJ, Chen GJ, Zhang HO, *et al*. 2020. Insights Into the role of exposed surface charged residues in the alkali-tolerance of GH11 xylanase. Front microbio. 11:872.
28. Li YY, Li C, Huang H, Rao SO, Zhang Q, Zhou JW, *et al*. 2022. Significantly enhanced thermostability of *Aspergillus niger* xylanase by modifying its highly flexible regions. J Agr Food Chem. 70:4620-4630.
29. Li TB, Yang SW, Wang XX, Cai HX, Wang Y, Li C, *et al*. 2022. Improving thermostability of GH11 xylanase XynASP by the design of loop region. Crystals. 12(9):1228.

30. Milos M, Jan S, Jaroslav B, Brezovsky Z, Prokop Z. 2017. FireProt: Web server for automated design of thermostable proteins. Nucleic Acids Res. 45:393-399.
31. Pornkanok P, Pratchaya W, Panu P. 2019. Identification of a hotspot residue for improving the thermostability of a flavin-dependent monooxygenase. Chem Bio Chem. 20(24):3020-3031.
32. Ashraf NM, Krishnagopal A, Hussain A, Kastner D, Sayed AMM, Mok K, *et al*. 2018. Engineering of serine protease for improved thermostability and catalytic activity using rational design. Int J Biol Macromol. 126:229-237.
33. Cheng Z, Lan Y, Guo J, Ma D, Jiang S, Lai Q, *et al*. 2020. Computational design of nitrile hydratase from *Pseudonocardia thermophila* JCM3095 for improved thermostability. Molecules. 25(20):1-18.
34. Liu Y, Li ZY, Guo C, Cui C, Wu ZL. 2021. Enhancing the thermal stability of ketoreductase ChKRED12 using the FireProt web server. Process Biochem. 101:207-212.
35. Hardy F, Vriend G, Veltman OR, van der Vinne B, Venema G, Eijsink VG. 1993. Stabilization of *Bacillus stearothermophilus* neutral protease by introduction of prolines. FEBS Lett. 317(2):89-92.
36. Yang WH, Yang YZ, Zhang LD, Xu H, Guo XJ, Yang X. 2017. Improved thermostability of an acidic xylanase from *Aspergillus sulphureus* by combined disulphide bridge introduction and proline residue substitution. Sci Rep. 7(1):1-9.
37. Kim T, Joo JC, Yoo YJ. 2012. Hydrophobic inter-action network analysis for thermostabilization of a mesophilic xylanase. J Biotechnol. 161(1):49-59.
38. Bhat SK, Purushothaman K, Kini KR, Gopala Rao Appu Rao AR. 2021. Design of mutants of GH11 xylanase from *Bacillus pumilus* for enhanced stability by amino acid substitutions in the N-terminal region: An *in silico* analysis. J Biomol Struct Dyn. 40(17):7666-7679.